Energy Technology
Generation, Conversion, Storage, Distribution
www.entechnol.de

Preparation of Electrolyte for Vanadium Redox-Flow Batteries Based on Vanadium Pentoxide

Jan Martin, Katharina Schafner, and Thomas Turek*

The vanadium redox-flow battery is a promising technology for stationary energy storage. A reduction in system costs is essential for competitiveness with other chemical energy storage systems. A large share of costs is currently attributed to the electrolyte, which can be significantly reduced by production based on vanadium pentoxide (V_2O_5). In this study, the dissolution kinetics of V_2O_5 in diluted sulfuric acid and commercial vanadium electrolyte (VE) is determined. The low solubility of V_2O_5 in sulfuric acid can be overcome by partially using VE with a state of charge of −50% as solvent. In this way, a complete dissolution of V_2O_5 is possible within ≈10 min to achieve the desired vanadium concentration of 1.6 mol L^{-1}. Moreover, the electrochemical reduction of an electrolyte containing VO_2^+ coupled with the oxygen evolution reaction at the anode is investigated. For these consecutive steps, an electrical energy demand of 1.69 kWh kg^{-1} is required to reach a state of charge of −50%. Finally, both processes are integrated into a plant concept for continuous electrolyte production.

1. Introduction

The negative environmental impact of carbon dioxide emissions from fossil fuels leads to a continuous expansion of renewable energies. In 2018, the share of renewable energies in gross electricity consumption in Germany was 37.8%,[1] and this share is to be increased to 80.0% by 2050.[2] However, renewable energy sources, such as wind and solar energy, are subject to considerable fluctuations, so storage technologies are required. These technologies must be able to store the energy during times of overproduction and feed it back into the power grid during peak loads, thus ensuring the stability of the grid, which is currently achieved by flexibly operated thermal power plants and pump storages.[3] With the rising share of renewable energy in electricity generation, however, additional energy storage facilities are necessary, especially for short-term storage.[4] An interesting technology for energy storage is the vanadium redox-flow battery (VRFB), which uses four stable oxidation stages of vanadium in the aqueous electrolyte (V^{2+}, V^{3+}, VO^{2+}, VO_2^+). This electrolyte is stored externally in two tanks and continuously conveyed through the cell.[5] However, commercialization is still inhibited by the high price of the electrolyte, which amounts to 31% of the total costs for a 10 kW/120 kWh system[6] and 43% for a 10 MW/40 MWh system.[7] During the discharge process, the reaction listed in Equation 1 takes place in the positive and Equation 2 in the negative electrolyte.[8] When charging, the two reactions take place in the opposite direction.

$$VO_2^+ + 2\,H^+ + e^- \rightleftharpoons VO^{2+} + H_2O \quad (1)$$

$$V^{2+} \rightleftharpoons V^{3+} + e^- \quad (2)$$

The most frequently used electrolyte mainly consists of vanadium ions dissolved in diluted sulfuric acid. The solubility of the vanadium ions strongly depends on the sulfuric acid concentration and the electrolyte temperature. For V^{2+}, V^{3+}, and VO^{2+}, an increase of the sulfuric acid concentration leads to a reduction of the solubility, but for VO_2^+ the solubility increases with rising H_2SO_4 concentrations.[9,10] The temperature dependence follows the opposite behavior. Here, the VO_2^+ solubility decreases with increasing electrolyte temperature, while the solubility of the other vanadium ions is enhanced.[9,10] The overall best total sulfuric acid concentration for a VRFB electrolyte is usually set to 2–2.5 mol L^{-1}.[10] A VRFB electrolyte with a total vanadium concentration of 1.6 mol L^{-1} and a total sulfate concentration of 4 mol L^{-1} is commercially available for instance from Gesellschaft für Elektrometallurgie mbH (GfE).[11] The optimum concentrations must be adapted to the ambient temperature of the VRFB site. Moreover, additives such as phosphoric acid or ammonium compounds are often added to the electrolyte.[12,13] These components serve as stabilizing agents and thus ensure that the VRFB can be operated in a broader temperature range.

Various vanadium-containing compounds can be used as educts for the production of the electrolyte. In the literature, mainly vanadium pentoxide V_2O_5, vanadyl sulfate $VOSO_4$, and partly also vanadium trioxide V_2O_3 are used. A summary of the production methods with these educts is given in **Table 1**. Interestingly, this is mainly patent literature; only very little information is available in the scientific literature.[9,10,14,15,19,24,28,34,35] V_2O_5 was selected for this study, as it is currently the only

J. Martin, K. Schafner, Prof. T. Turek
Institute of Chemical and Electrochemical Process Engineering
Clausthal University of Technology
38678 Clausthal-Zellerfeld, Germany
E-mail: martin@icvt.tu-clausthal.de

The ORCID identification number(s) for the author(s) of this article can be found under https://doi.org/10.1002/ente.202000522.

DOI: 10.1002/ente.202000522

Table 1. Comparison of published production processes for VRFB electrolyte.

Educt(s)	Oxidation reaction	Reduction reaction	Solvent	Source
Electrochemical reduction				
V_2O_5	$H_2O \rightleftharpoons 0.5O_2 + 2H^+ + 2e^-$	$2VO_2^+ + 3e^- + 6H^+ \rightleftharpoons VO^{2+} + V^{3+} + 3H_2O$	H_2SO_4	[14-18]
$VOSO_4$	$VO^{2+} + H_2O \rightleftharpoons VO_2^+ + e^- + 2H^+$	$VO^{2+} + 2e^- + 2H^+ \rightleftharpoons V^{2+} + H_2O$	H_2SO_4	[10,19,20]
$VOSO_4$	$VO^{2+} + H_2O \rightleftharpoons VO_2^+ + e^- + 2H^+$	$VO^{2+} + e^- + 2H^+ \rightleftharpoons V^{3+} + H_2O$	H_2SO_4	[21,22]
$VOSO_4$	$H_2 \rightleftharpoons 2H^+ + 2e^-$	$2VO^{2+} + e^- + 2H^+ \rightleftharpoons VO^{2+} + V^{3+} + H_2O$	H_2SO_4	[23]
$VOCl_3$	$H_2O \rightleftharpoons 0.5O_2 + 2H^+ + 2e^-$	$2VO_2^+ + 3e^- + 6H^+ \rightleftharpoons VO^{2+} + V^{3+} + 3H_2O$	H_2SO_4	[24]
Chemical reduction				
V_2O_5	$SO_2 + 2H_2O \rightleftharpoons H_2SO_4 + 2e^- + 2H^+$	$VO_2^+ + e^- + 2H^+ \rightleftharpoons VO^{2+} + H_2O$	H_2SO_4	[25-27]
V_2O_5	$C_2H_2O_4 \rightleftharpoons 2CO_2 + 2e^- + 2H^+$	$VO_2^+ + e^- + 2H^+ \rightleftharpoons VO^{2+} + H_2O$	H_2SO_4	[15,25,26]
$VOSO_4$	$CH_2O_2 \rightleftharpoons CO_2 + 2e^- + 2H^+$	$VO^{2+} + e^- + 2H^+ \rightleftharpoons V^{3+} + H_2O$	H_2SO_4	[28]
V_2O_5	$H_2SO_3 + H_2O \rightleftharpoons H_2SO_4 + 2e^- + 2H^+$	$VO_2^+ + e^- + 2H^+ \rightleftharpoons VO^{2+} + H_2O$	H_2SO_4	[29]
$VOSO_4$	$H_2 \rightleftharpoons 2H^+ + 2e^-$	$VO^{2+} + e^- + 2H^+ \rightleftharpoons V^{3+} + H_2O$	H_2SO_4	[25,26]
V_2O_3	$V^{3+} + H_2O \rightleftharpoons VO^{2+} + e^- + 2H^+$	$VO_2^+ + e^- + 2H^+ \rightleftharpoons VO^{2+} + H_2O$	H_2SO_4	[30-32]
V_2O_5	$S + 2H_2O \rightleftharpoons SO_2 + 4e^- + 4H^+$	$VO_2^+ + 2e^- + 4H^+ \rightleftharpoons V^{3+} + 2H_2O$	Solid mixing	[9,25,33]
$VOSO_4$	$S + 2H_2O \rightleftharpoons SO_2 + 4e^- + 4H^+$	$VO^{2+} + e^- + 2H^+ \rightleftharpoons V^{3+} + H_2O$	Solid mixing	[9,25,33]
V_2O_5	$0.5H_2O_2 \rightleftharpoons H^+ + e^- + 0.5O_2$	$VO_2^+ + e^- + 2H^+ \rightleftharpoons VO^{2+} + H_2O$	H_2SO_4	[34]
Dissolution of precursors				
VCl_3, $VOSO_4$	$VOSO_4 \rightleftharpoons VO^{2+} + SO_4^{2-}$	$VCl_3 \rightleftharpoons V^{3+} + 3Cl^-$	H_2SO_4	[24,35]

starting material suitable for large-scale production with a price of around €11 kg^{-1}.[36,37] The price is mainly determined by the steel industry, as V_2O_5 is a precursor of ferro-vanadium.[38,39] A challenge with V_2O_5 is the significantly lower solubility, for example in comparison with $VOSO_4$. At the industrial conditions of the electrolyte and a temperature of 20 °C, the solubility of the corresponding VO_2^+ ions is only 0.5 mol L^{-1}.[40] Therefore, a reduction of the pentavalent vanadium ions is necessary to increase the total vanadium concentration to the required 1.6 mol L^{-1}. Two fundamentally different possibilities are available for this, namely, chemical and electrochemical reduction. During chemical reduction, the tetra- or pentavalent vanadium component is reduced with chemical reducing agents such as sulfur dioxide SO_2,[25] oxalic acid $C_2H_2O_4$,[24] or hydrogen H_2.[24,25] In electrochemical reduction, the vanadium ions are continuously reduced with the aid of electric current. Various oxidation reactions at the anodic half-cell can be applied, such as the oxygen evolution reaction[14,16–18] or the oxidation of hydrogen.[23] The aim of this work is to develop a process that continuously produces a vanadium electrolyte (VE) with a composition identical to that of commercially available electrolytes. For this purpose, the most relevant steps, i.e., the dissolution of V_2O_5 in different solvents and the consecutive electrochemical reduction, are investigated separately. Finally, these two steps are combined into one concept for a continuous process.

2. Experimental Section

2.1. Materials

The chemicals applied were V_2O_5 from GfE with two different sieve fractions with nominal diameters d_{90} of 50 and 300 µm and a purity of 99.6%. The particle size distribution of both materials is examined in the following section. H_2SO_4 from Carl Roth and deionized water, which was produced with a MilliQ system by Millipore, were used. Moreover commercial VE was acquired from GfE with an equimolar ratio of V^{3+} and VO^{2+}. The electrolyte consists of 1.6 mol L^{-1} total vanadium and 4 mol L^{-1} total sulfate concentration. The total vanadium concentration and the state of charge (SoC) of the electrolyte were measured with redox titration by a Titrando 888 of Metrohm AG. Therefore the positive electrolyte was reduced with an ammonium iron(II) sulfate solution. Then, potassium permanganate was inserted into the positive and negative electrolyte and the potential was continuously recorded. Further details can be found in the literature.[41,42]

2.2. Experiments

2.2.1. Particle Size Distribution

The particle size distribution measurements were conducted with a QICPIC particle size analyzer of Sympatec GmbH. A size range of 5–1700 µm was selected for the measurements. The number of particles measured varied between 50 000 and 70 000. Three measurements were taken for each material, which were then averaged. Prior to the analysis, the particles had been dispersed with a RODOS/L dry dispersion unit, also of Sympatec GmbH.

2.2.2. Dissolution Experiments

The solution kinetics were investigated for the two vanadium pentoxide sieve fractions in different solvents. Solid (1.445 g)

was mixed at room temperature, which was in the range of 20–25 °C, with 10 mL solvent under stirring by a magnetic stirrer at a constant speed of 400 min^{-1} for different periods of time in the range from 2 min up to 24 h. The ratio of solid and solvent was adjusted in such a way that a total vanadium concentration of 1.6 mol L^{-1} was obtained after complete dissolution. After the required dissolution time, the suspension was filtered using a paper filter and the vanadium concentration and the SoC were determined by redox titration. The SoC is defined as the quotient of the concentration of the charged species VO_2^+ and the absolute concentration of vanadium ions in the positive electrolyte, according to Equation (3).

$$SoC_{PE} = \frac{c_{VO_2^+}}{c_{VO_2^+} + c_{VO^{2+}}} \tag{3}$$

The solution kinetics of both particle size distributions were first examined in sulfuric acid with a concentration of 4 mol L^{-1} as solvent. In addition, a mixture of different ratios of sulfuric acid with the same concentration and commercial VE was used as solvent. This represents the more realistic application for the operation of a continuous plant. The two volumetric solvent ratios examined were H_2SO_4/VE of 2/1 and 1/2. The dissolution experiments with mixtures of sulfuric acid and VE were conducted with a nominal particle diameter of 50 µm. When calculating the required V_2O_5 mass, it must be ensured that the total vanadium concentration at complete dissolution is 1.6 mol L^{-1}. The dissolved fraction of V_2O_5 w_{Sol} can be calculated using Equation (4).

$$w_{Sol} = \frac{(c_V - c_{V.0}) \cdot M_{V_2O_2} \cdot V_S}{2 \cdot \rho_{V_2O_5}} \tag{4}$$

Here the concentrations refer to the total concentration of vanadium with all oxidation states, $c_{V.0}$ is the vanadium concentration at time 0, caused by the VE, while V_S describes the volume of the solvent applied.

2.2.3. Electrochemical Reduction

For the investigation of the electrochemical reduction the same commercially available electrolyte from GfE was applied. Before the experiments, the electrolyte has to be charged to an SoC of 100%. The cell for electrochemical reduction is shown in **Figure 1**.

The cathode material used was a GFD 4.6 EA type carbon felt from SGL Carbon SE that was thermally activated at 400 °C for 6 h and was compressed to half its thickness through the additional midframe. As anode material an IrO_2-coated titanium plate was applied, because IrO_2 has the second highest electrochemical activity for oxygen evolution in acidic environments and is more stable compared to ruthenium.[43] A Nafion117 membrane was used to separate the two half-cells. Prior to the measurements, the membrane was immersed in 1 wt% sulfuric acid for 12 h. Gold-plated nickel nets were used as current conductors at both electrodes. The end-frames were made of polymethylmethacrylate and had a total of six holes through which the cell could be fixed using screws and nuts. This ensures uniform compression of the cell. Two additional

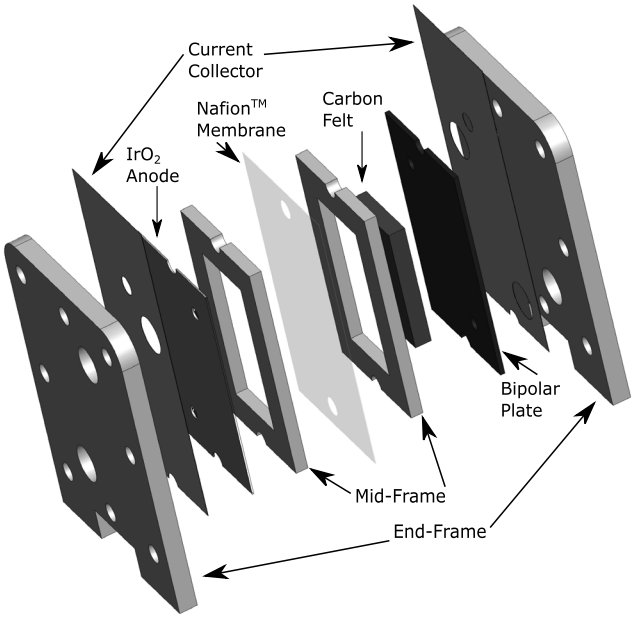

Figure 1. Schematic design of the applied electrolysis cell.

frames in the middle of the cell limited the active electrode areas to 10 cm^2 each. Silicone seals were used between the individual components to seal the cell; these are not shown in Figure 1 for simplicity. The VE was continuously pumped through the cathode with a volume flow rate of 3.5 mL s^{-1} using a type NF 1.25 membrane pump of KNF Neuberger GmbH. On the anode side, sulfuric acid with a concentration of 4 mol L^{-1} was used as electrolyte. Thus water was oxidized to oxygen at the anode; the conductivity of the electrolyte was increased by the protons in the solution, which reduced the ohmic losses. The use of diluted sulfuric acid prevented the crossover of foreign ions to the cathode side. Each reaction was conducted until an SoC of −50% was reached. Therefore, the SoC was analyzed with redox titration every 30 min. When all VO_2^+ ions were consumed due to the reduction, the SoC had to be determined according to the method for the negative electrolyte. The cell voltage was measured in a time interval of 5 s with an Interface 1000 potentiostat from Gamry Instruments. The reaction conditions considered are summarized in **Table 2**.

The temperature on the cathode side was controlled by a thermostat and a water bath. Room temperature was used on the anode side, which was in the range of 20–25 °C. The specific electrical energy requirement E for the electrolyte production for each experiment was then determined using Equation (5).

Table 2. Reaction conditions investigated for the characterization of the electrochemical reduction.

No.	Current density [mA cm^{-2}]	Catholyte temperature [°C]
1	100	20
2	50	20
3	50	30

Thereby the measured values were added up over the measuring interval of 5 s.

$$E = \frac{\sum_{t=0}^{t_R} (U_C \cdot I_C \cdot \Delta t)}{n_V(t) \cdot M_V} \tag{5}$$

Here, U_C is the measured cell voltage, I_C the corresponding current, n_V the total amount of vanadium in the electrolyte at the respective time, and M_V the molar mass of the vanadium. The volume reduction of 0.5 mL for the determination of the SoC every 30 min was also taken into account.

2.3. Dissolution Kinetics

2.3.1. Nernst–Brunner Dissolution Model

The Nernst–Brunner equation as a simple diffusion layer model was used to describe the dissolution kinetics.[44] The model assumes that a stagnant boundary film of constant thickness exists around the particle. Within that film mass transport is only achieved by means of Fickian diffusion.[45] Directly at the particle surface, the saturation concentration c_{Sol} is present. For V_2O_5 dissolved in sulfuric acid with a concentration of 4 mol L^{-1} at standard temperature, the solubility is approximately 0.5 mol L^{-1}.[40] The boundary film is in contact with the ideally mixed liquid bulk. The Nernst–Brunner equation, resulting from this model conception, is listed in Equation (6).[46]

$$\frac{dc_V}{dt} = \frac{D_{VO_2^+} \cdot \sum_i (\Delta Q_{3,i} \cdot S_{P,i} \cdot N_{P,i})}{\delta \cdot V_S} \cdot (c_{sol} - c_V) \tag{6}$$

The particle size distribution was included with different particle size fractions, which is described with the distribution $\Delta Q_{3,i}$. The model considered that the particles are spherical, the amount of particles $N_{P,i}$ in every size class remained constant, and the diffusion coefficient $D_{VO_2^+}$ is independent of the film thickness. Moreover, the model assumed that the particle surface area $S_{P,i}$ of each size class did not change during the solution process. However, this was a simplification that deviates greatly from reality and is only valid if the solid is present in excess. As in this work the V_2O_5 should be dissolved completely, the Nernst–Brunner equation was extended in the following taking the surface reduction into account. Therefore, the surface area $S_{P,i}$ was expressed as a function of the particle diameter as shown in Equation (7).

$$S_{P,i} = \pi \cdot \left(d_{0,i}^2 - d_i^2\right) \tag{7}$$

Furthermore the particle diameter d_i can be expressed in dependence of the bulk concentration c as shown in Equation (8).

$$d_i = \sqrt[3]{\frac{6 \cdot M_{V_2O_5} \cdot V_S \cdot c}{\rho_{V_2O_5} \cdot \pi \cdot N_{P,i}}} \tag{8}$$

With these equations, the Nernst–Brunner equation including the changing particle surface area can be expressed as shown in Equation (9).

$$\frac{dc_V}{dt} = \frac{D_{VO_2^+} \cdot \pi \cdot \sum_i \left(\Delta Q_{3,i} \cdot N_{P,i} \left(d_{0,i}^2 - \left(\frac{6 M_{V_2O_5} V_S c_V}{\rho_{V_2O_5} \pi N_{P,i}}\right)^{\frac{2}{3}}\right)\right)}{\delta \cdot V_S} \cdot (c_{sol} - c_V) \tag{9}$$

Both equations can be adapted to the measurement results of the dissolution kinetics by adjusting the film thickness δ.

2.3.2. Empirical Estimation of Film Thickness

For comparison, the film thickness δ was additionally calculated with a state-of-the-art Sherwood correlation; see Equation (10).[47] The film thickness was then derived from the quotient of the diffusion coefficient and the mass transfer coefficient.

$$Sh = \frac{\beta \cdot d_P}{D_{VO_2^+}} = 2 + 0.5 \cdot \left(\frac{\varepsilon^{\frac{1}{3}} \times d_P^{\frac{4}{3}}}{\nu_{Sus}}\right)^{0.62} Sc^{\frac{1}{3}} \tag{10}$$

In this equation, ε describes the energy dissipation rate, which can be determined with Equation (11).[48]

$$\varepsilon = \frac{Ne \times n^3 \times d_{Stir}^5}{V_{V_2O_5} + V_S} \tag{11}$$

Furthermore, the Newton number Ne was required, which takes the dimensionless mechanical energy input of the stirrer into account. For a blade stirrer, the relationship given in Equation (12) was developed.[49] The cylindrical magnetic stirrer used in the experiments can be compared in good approximation with a blade stirrer.

$$Ne = \frac{1}{Re^{0.1}} \tag{12}$$

The stirrer blade to tank ratio of 0.33 in the experimental set-up was in good agreement with the value of 0.4 applied in the correlation. To describe the density and viscosity of the suspension, the following expressions were used in Equation (13) and (14).[50]

$$\rho_{Sus} = \varphi \times \rho_{V_2O_5} + (1 - \varphi)\rho_{H_2SO_4} \tag{13}$$

$$\eta_{Sus} = \eta_{H_2SO_4} \left(1 + \frac{2.5\,\varphi}{2\left(1 - \frac{\varphi}{\varphi_{max}}\right)}\right)^2 \tag{14}$$

The factor φ describes the fraction of the solid matter and can be taken from Equation (15).

$$\varphi = \frac{V_{V_2O_5}}{V_{V_2O_5} + V_S} \tag{15}$$

The maximum volume fraction of a packed bed of spheres φ_{max} can be calculated to 0.74.

3. Results and Discussion

3.1. Particle Size Distribution

The particle size distributions for both applied vanadium pentoxide powders are shown in **Figure 2**. The left diagram of Figure 2 contains the particle size distribution of the V_2O_5 powder with a nominal diameter d_{90} of 300 µm. A broad distribution in the range between 50 and 400 µm can be observed. The measured d_{90} value of 350 µm deviates ≈15% from the nominal value. The right diagram of Figure 2 shows a more narrow distribution for the nominal 50 µm particles. The measured d_{90} value for this size fraction is 60 µm. Both particle size distributions are slightly larger than declared. In the following sections, the particle size distributions are nevertheless still referred to as 50 and 300 µm for clarification.

3.2. Dissolution Kinetics

3.2.1. Influence of Particle Diameter

The concentrations for the dissolution of V_2O_5 with the two different particle diameters in diluted sulfuric acid as solvent as a function of time are shown in **Figure 3**. As VO_2^+ ions cannot be reduced in sulfuric acid, the resulting SoC of the solution is constantly maintained at 100%; therefore, the VO_2^+ concentration is shown.

For both particle sizes, the concentration in the solution increases rapidly in the first 30 min, as there is a large concentration difference between the particle and the bulk solution. As these concentrations approach, the curves continue to flatten until after about 3 h the saturation concentration of 0.5 mol L^{-1} is reached for both fractions, which is also plotted with a dashed line in the diagram.[40] In the right area of Figure 3, the first 30 min is shown in detail. It can be observed that the concentration of the VO_2^+ ions for the smaller particles is slightly higher at any time and that they are thus better suited for electrolyte production. This can be explained with the higher total surface area of these particles, which is available for dissolution. However, after a dissolution time of approximately 1 h, the concentrations are almost identical. The influence of the particle size on the dissolution kinetics can be no longer detected. This can be explained with the shrinking driving force for dissolution. Furthermore, the error bars of the measurements can be seen in Figure 3. These are the standard deviations of the three tests performed for each time interval. A good reproducibility of the measurements is achieved; the standard deviation of the measured concentration is on average only 0.01 mol L^{-1} and thus in the error range of the concentration measurement. Overall, it can be derived from the experiments that a higher surface area accelerates the dissolution kinetics until a VO_2^+ concentration in the solution of roughly 0.4 mol L^{-1} is reached. The concentration profiles obtained are in good agreement with recent findings by El Hage et al.[51] In this work, V_2O_5 was dissolved in 3 M sulfuric acid. At 25 °C, a VO_2^+ concentration of ≈0.42 mol L^{-1} was reached after 1 h, while the saturation concentration of 0.5 mol L^{-1} was reached after 3 h.

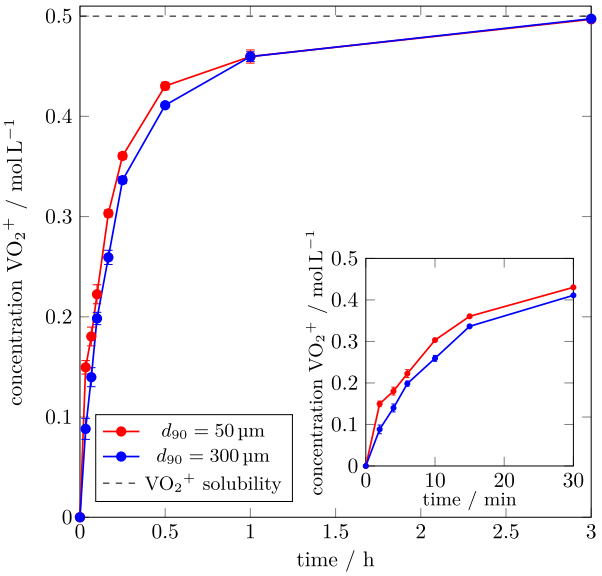

Figure 3. Influence of particle size of vanadium pentoxide on the solution kinetics with diluted sulfuric acid as solvent at 20 °C; the insert shows magnification for the first 30 min.

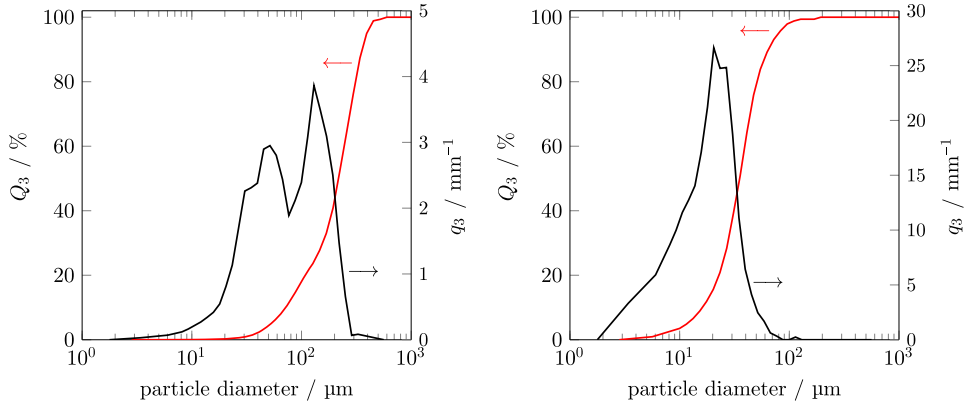

Figure 2. Cumulative particle size distribution (red) and density particle size distribution (black) of the applied V_2O_5 materials. Left nominal diameter $d_{90} = 300$ µm, right nominal diameter $d_{90} = 50$ µm.

3.2.2. Adaptation of the Nernst–Brunner Equation

The concentration profiles calculated with the Nernst–Brunner equation are shown in **Figure 4**. The values of all material data used for the calculation are listed in **Table 3**. It can be recognized from the diagrams that both models can precisely predict the concentration of the solution in the first 20 min. In the following time, only the consideration of the shrinking surface area ensures a correct prediction of the film thickness, whereas the solution kinetics are predicted too fast without this effect. At the end of the investigated time, the concentrations approach again.

3.2.3. Evaluation of the Film Thickness

Table 4 compares the film thicknesses, on the one hand adjusted with the Nernst–Brunner equations and on the other hand calculated with the Sherwood correlation discussed in Section 2.3. Values for the material data and dimensions applied, which are required for the theoretical determination, are listed in **Table 5**.

For the 300 µm particles, a relatively good agreement between the different values can be recognized; the values deviate only slightly from the empirical value. However, for the smaller particles the deviations increase significantly. When considering the reduced surface area while dissolving, the determined film thickness reduces to 60.7 µm. Nevertheless, this value is still larger by a factor of 6 compared to the empirical film thickness determined with the Sherwood correlation. These deviations might be explained with either agglomeration of the V_2O_5 particles or adhesions on the wall. Both effects drastically reduce the total surface area, which directly decreases the dissolution rate. The theoretically estimated film thicknesses can be confirmed with values from the literature for dissolving under stirring; these are often assumed to be in the range of 5–20 µm.[53,54] Furthermore, the fact that the film thickness decreases with shrinking particle sizes can be found in the literature as well.[53] This behavior cannot be described with the Nernst–Brunner equations, because the film thickness increases for the 50 µm particles.

Table 3. Parameters for the Nernst–Brunner equation.

Parameter	Value	Unit
$D_{VO_2^+}$	3.9×10^{-10}[52]	$m^2\,s^{-1}$
c_S	0.5	$mol\,L^{-1}$
V_S	10	mL
$\rho_{V_2O_5}$	3360	$kg\,m^{-3}$
$M_{V_2O_5}$	181.88	$g\,mol^{-1}$

Table 4. Comparison between film thicknesses calculated with the Nernst–Brunner equation and empirically determined with the Sherwood correlation.

Diameter [µm]	Const. surface [µm]	Shrinking surface [µm]	Sh correlation [µm]
300	30.7	11.7	17.8
50	151.9	60.7	9.8

Table 5. Parameters for the film thickness determination.

Parameter	Value	Unit
$m_{V_2O_5}$	1.445	g
$V_{V_2O_5}$	4.33×10^{-4}	L
$\rho_{H_2SO_4}$	1235	$kg\,m^{-3}$
$\eta_{H_2SO_4}$	0.005	Pa s
d_{Stir}	20	mm
d_{Tank}	50	mm
n	400	min^{-1}
φ_{max}	0.74	–

3.2.4. Influence of Solvent Ratio

Three different solvent ratios are examined, while the results for diluted sulfuric acid are already provided in Section 3.2.1. The development of the concentrations as a function of time is shown in **Figure 5**. The dissolution in diluted sulfuric acid shown in blue reaches equilibrium after ≈1 h. Only a quarter

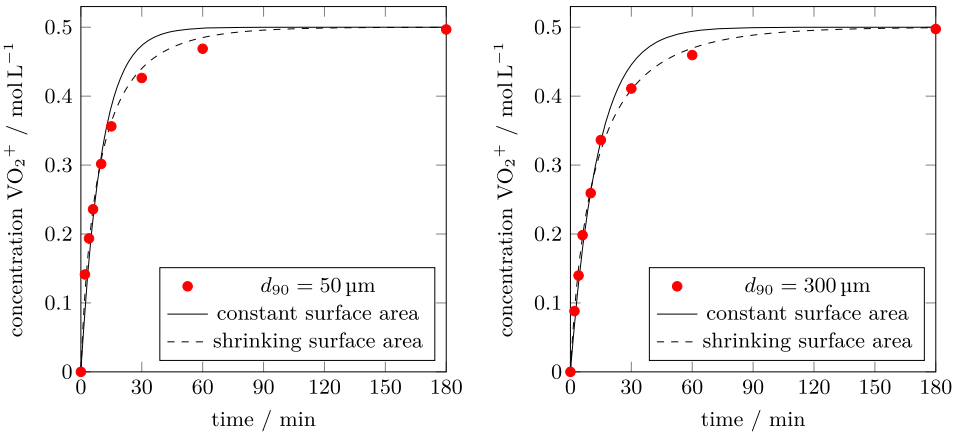

Figure 4. Model adaptation of the Nernst–Brunner equation to the dissolution kinetics of the 50 µm particles (left) and the 300 µm particles (right).

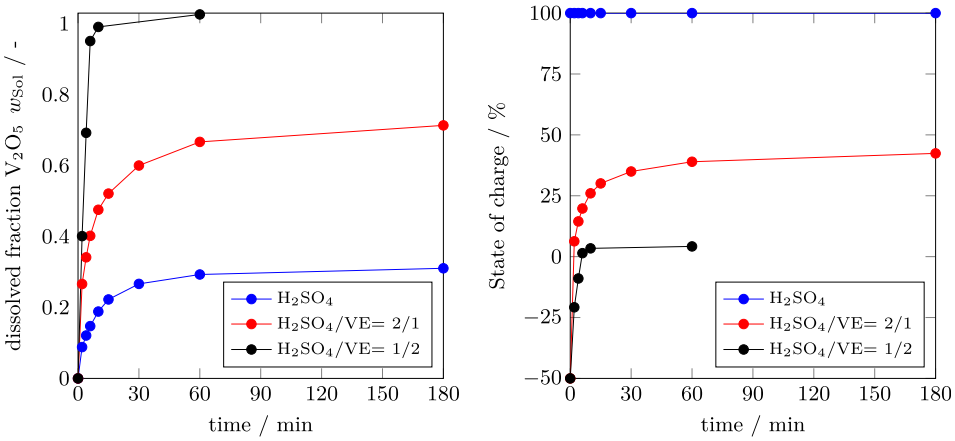

Figure 5. Influence of the solvent ratio H_2SO_4/VE on the solution kinetics of V_2O_5 particles with a particle size of 50 µm at room temperature.

of the vanadium pentoxide can be dissolved due to the limited solubility. The SoC maintains a constant value of 100%, as only VO_2^+ ions dissolve. The H_2SO_4/VE mixtures have an SoC of −50% at the start of the reaction, as this is determined by the added proportion of the VE. Commercial VE contains an equimolar ratio of V^{3+} and VO^{2+}, which corresponds to an SoC of −50%. The contained V^{3+} ions accelerate the dissolution by chemical reduction of the VO_2^+, as shown in Equation (16).

$$VO_2^+ + V^{3+} \rightleftharpoons 2\,VO^{2+} \tag{16}$$

Therefore, a high driving force for the dissolution is maintained, because the dissolved VO_2^+ ions are reduced to VO^{2+} by the V^{3+} ions of the VE. This also explains why the initial gradients are maintained for longer in experiments with solvent mixtures. The use of one-third VE as solvent causes about 70% of the deployed V_2O_5 to be dissolved. The final SoC of ≈45% indicates that all V^{3+} ions are oxidized and solubility in regard to the VO_2^+ ions is reached, as its concentration in the solution is ≈0.5 mol L^{-1}. Almost no further increase of the dissolved fraction can be detected after 1 h of dissolution time. When using two-thirds of VE as solvent, the complete V_2O_5 fraction is dissolved in ≈10 min. Obviously, the dissolution rate is significantly higher than in the other experiments. The final SoC of about 5% indicates that mainly VO^{2+} ions are present in the solution. In conclusion, the target concentration of 1.6 mol L^{-1} can only be achieved if VE is added in excess.

3.3. Electrochemical Reduction

Figure 6 shows the cell voltage as a function of the dimensionless time in dependence of the current density in the top left diagram and for different catholyte temperatures in the bottom left diagram. The dimensionless time is the current reduction time normalized to the total reaction time, which was ≈3 h in each experiment. The corresponding profiles of the SoC are shown on the right side of Figure 6, respectively.

Two characteristic areas are recognizable in the cell voltage profiles. Up to the dimensionless time of ≈0.6−0.65, the voltage rises steadily. The reason for this is that the VO_2^+ ions present in the electrolyte are first reduced to tetravalent vanadium ions. This reaction has an equilibrium potential of 1.00 V under standard conditions.[55] Thus, a reversible standard cell voltage of the electrolysis cell of 0.23 V is obtained, as the oxygen evolution reaction at the anode requires 1.23 V. The difference to this theoretical value is caused by the different overpotentials in the system. As soon as all pentavalent vanadium ions are consumed, the formed VO^{2+} ions are further reduced to V^{3+} ions. The standard equilibrium potential of this reaction is 0.34 V.[56] This results in a higher reversible standard cell voltage of 0.89 V, which explains the abrupt increase in cell voltage. The overpotentials can be determined from the difference between the cell voltage and the equilibrium voltage. From the top left figure, it can be seen that at twice the current density the overpotential is around 200 mV higher. Furthermore, it can be seen that the kinetics for the reduction of VO^{2+} ions are worse compared to the reduction of pentavalent vanadium ions. At a current density of 100 mA cm^{-2}, the corresponding values for the overpotential of VO^{2+} and VO_2^+ reduction are ≈1200 and 600 mV. As this reaction is more important for continuous electrolyte production, research to diminish this overpotential has to be conducted. The corresponding profiles of the SoC show an almost linear decrease, which is caused by the applied constant current. Only at a current density of 50 mA cm^{-2} is the drop in the first 30 min higher than expected. This effect was taken into account when determining the energy requirement *E*, by adding an additional theoretical reaction time for this decrease.

In the bottom left part of Figure 6, a slightly decreasing cell voltage at higher catholyte temperature can be observed. Over the entire reaction time, the cell voltage is reduced by ≈50 mV. However, an increase of the catholyte temperature to over 40 °C is not possible, as the VO_2^+ ions are then no longer stable in the aqueous solution.[10] An increase of the anolyte temperature should also be considered to reduce the cell voltage in future work, as the oxygen evolution reaction is known to have high overpotentials.[57] The electrical energy demands of the electrolysis cell can be calculated according to Equation (5), and the obtained values are summarized in **Table 6**. For the calculation, energy requirements of peripheral devices are not taken into account.

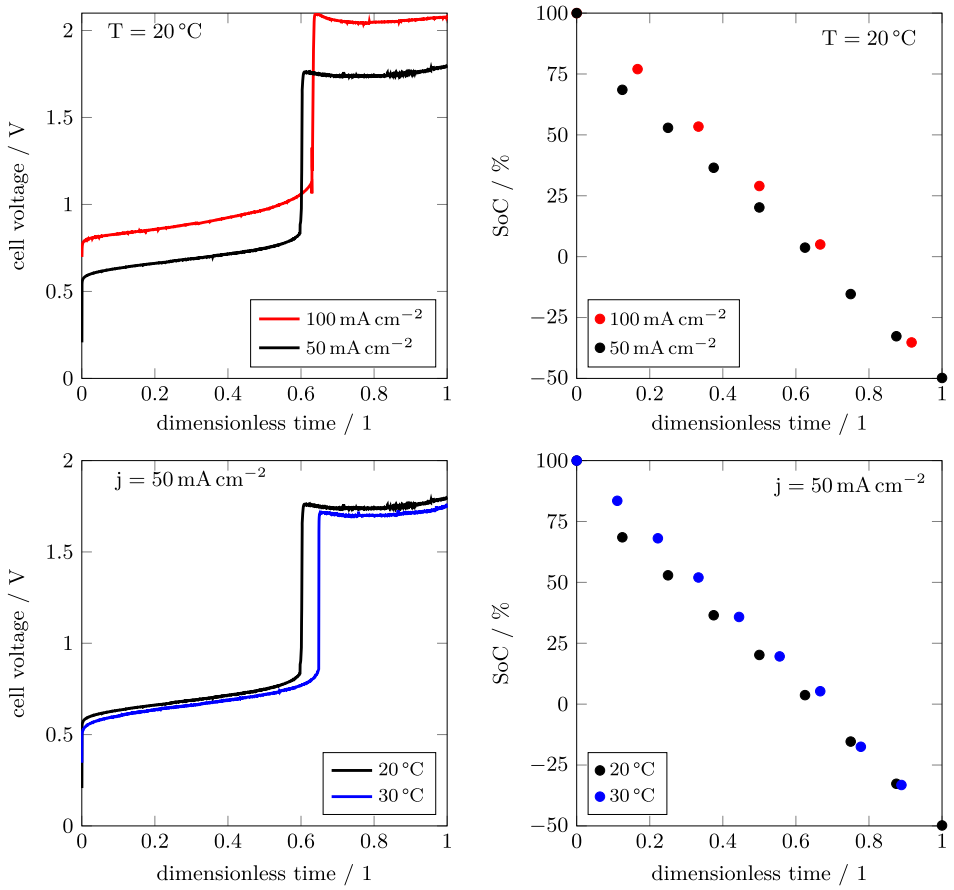

Figure 6. Cell voltage as a function of dimensionless time in dependence of current density (top left) and catholyte temperature (bottom left) with the corresponding SoC (top right and bottom right).

Table 6. Calculated electrical energy demands for the different test conditions.

Experimental conditions	Electrical energy demand [kWh kg^{-1}]
100 mA cm^{-2}, 20 °C	2.03
50 mA cm^{-2}, 20 °C	1.80
50 mA cm^{-2}, 30 °C	1.69

It can be recognized that the electrical energy requirement for electrolyte production at 20 °C is 0.23 kWh kg^{-1} lower for the current density of 50 mA cm^{-2}, compared to 100 mA cm^{-2}. This is mainly due to the lower overpotentials, as these depend linearly on the current density. For technical applications, however, twice the amount of electrolyte can be produced with an ≈10% higher energy requirement. Increasing the catholyte temperature by 10 °C leads to a further reduction of the energy requirement by 0.11 kWh kg^{-1}. With a typical industrial electricity price of €0.06 kWh^{-1} in Germany, the cost of electrochemical reduction is €0.1 kg^{-1}, which is only ≈10% of the raw material cost of V_2O_5 kg^{-1} electrolyte. This shows that the process is dominated by raw material costs. In addition, commercial VE can currently be purchased for a price of about €4 kg^{-1}.[11] In contrast, the raw material costs of $VOSO_4$ are currently about €3 kg^{-1} electrolyte.[58]

4. Conclusions

In this study, the dissolution kinetics of V_2O_5 in diluted sulfuric acid with a concentration of 4 mol L^{-1} and mixtures of diluted sulfuric acid and VE are investigated. V_2O_5 is selected as a starting material for electrolyte production because of its low price and high availability. Moreover, the electrochemical reduction of VO_2^+ was studied with the oxygen evolution reaction at the anode. It could be shown that when applying VE as solvent in excess, a total dissolution of the V_2O_5 is reached within a dissolution time of approximately 10 min, achieving a total vanadium concentration of 1.6 mol L^{-1}. The specific energy demand of the electrochemical reduction could be reduced to 1.69 kWh kg^{-1} at a current density of 50 mA cm^{-2} by applying a catholyte temperature of 30 °C. Further decreases of the energy demand could be achieved by heating the anolyte as well. For a continuous electrolyte production for VRFB, these two processes have to be combined to a single plant. As the dissolution equilibrium of VO_2^+ with 0.5 mol L^{-1} is considerably below the required vanadium concentration in the electrolyte of 1.6 mol L^{-1}, a plant concept is developed. The schematic drawing of this is shown in **Figure 7**.

The concept consists of a stirred mixing vessel into which vanadium pentoxide and diluted sulfuric acid are continuously dosed. For sulfuric acid dosing, it must be taken into account that the dissolution of V_2O_5 is proton-consuming. An overflow

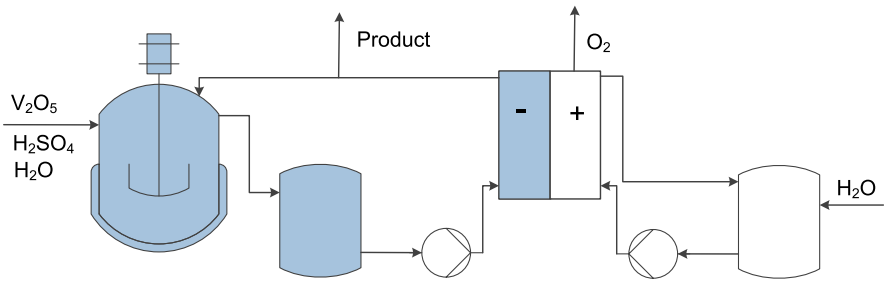

Figure 7. Schematic drawing of a plant concept for continuous electrolyte production.

ensures the liquid transfer from the mixing vessel into a second tank. For complete solid retention, a filter is additionally added between the two containers. From the second tank, the solution is pumped into the cathode of the electrochemical cell and after reduction returned to the stirred mixing tank. However, a partial flow is continuously discharged as product stream. The volume flow of that stream is directly coupled with the current in the electrochemical cell. Therefore, an SoC of −50% can be reached for the product stream. For example, a conductivity measurement can serve as an additional control of a constant product composition. As the solid V_2O_5 is retained in the stirred mixing vessel, porous carbon felts can be used as electrode material at the cathode. These minimize the cell voltage and thus the energy required for the electrolyte production. In addition, the recirculation of the V^{3+} ions causes an accelerated dissolution of the pentavalent vanadium ions in the mixing vessel due to chemical reduction. This effect was also investigated in the presented experiments. On the anode side, diluted sulfuric acid is conveyed through the cell from a storage tank. Due to the oxygen evolution reaction in the electrochemical cell, water has to be added continuously to the anode storage tank. For a high energy efficiency noble metal electrocatalysts, for example, the IrO_2 used in this study, should be applied as anode materials to reduce the cell voltage.

Acknowledgements

The authors gratefully acknowledge thyssenkrupp Industrial Solutions AG for financial support and the supply of the IrO_2 electrode. Open access funding enabled and organized by Projekt DEAL.

Conflict of Interest

The authors declare no conflict of interest.

Keywords

dissolution kinetics, electrochemical reduction, electrolyte production, vanadium pentoxide, vanadium redox-flow batteries

Received: June 4, 2020
Revised: July 16, 2020
Published online: August 7, 2020

[1] H.-K. Bartholdsen, A. Eidens, K. Löffler, F. Seehaus, F. Wejda, T. Burandt, P.-Y. Oei, C. Kemfert, C. von Hirschhausen, *Energies* **2019**, *12*, 2988.
[2] N. Szarka, M. Eichhorn, R. Kittler, A. Bezama, D. Thrän, *Renewable Sustainable Energy Rev.* **2017**, *68*, 1222.
[3] A. Evans, V. Strezov, T. J. Evans, *Renewable Sustainable Energy Rev.* **2012**, *16*, 4141.
[4] M. Sterner, I. Stadler, *Handbook of Energy Storage: Demand, Technologies, Integration*, Springer, Berlin **2018**.
[5] M. Rychcik, M. Skyllas-Kazacos, *J. Power Sources* **1988**, *22*, 59.
[6] J. Noack, L. Wietschel, N. Roznyatovskaya, K. Pinkwart, J. Tübke, *Energies* **2016**, *9*, 627.
[7] C. Minke, U. Kunz, T. Turek, *J. Power Sources* **2017**, *361*, 105.
[8] W. Wang, Q. Luo, B. Li, X. Wei, L. Li, Z. Yang, *Adv. Funct. Mater.* **2013**, *23*, 970.
[9] M. Skyllas-Kazacos, L. Cao, M. Kazacos, N. Kausar, A. Mousa, *ChemSusChem* **2016**, *9*, 1521.
[10] K. Wang, Y. Zhang, J. Le Liu, *Electrochim. Acta* **2018**, *259*, 11.
[11] Vanadium Electrolyte Solution – Gesellschaft für Elektrometallurgie mbH, https://bit.ly/2WBNSKC (accessed: April 2020).
[12] K.-L. Huang, S.-Q. Liu, N. Tan, L.-Q. Chen, *Renewable Energy* **2008**, *33*, 186.
[13] L. Cao, M. Skyllas-Kazacos, C. Menictas, J. Noack, *J. Energy Chem.* **2018**, *27*, 1269.
[14] M. Kazacos, M. Cheng, M. Skyllas-Kazacos, *J. Appl. Electrochem.* **1990**, *20*, 463.
[15] C. Choi, S. Kim, R. Kim, Y. Choi, S. Kim, H.-y. Jung, J. H. Yang, H.-T. Kim, *Renewable Sustainable Energy Rev.* **2017**, *69*, 263.
[16] M. Skyllas-Kazacos, M. Kazacos, WO 1989/005363A1, **1988**.
[17] B. M. Broman, A. Pellegri (Squirrel Holdings Ltd.), WO 2002/015317, **2002**.
[18] M. Kazacos, M. Skyllas-Kazacos, (I. VRB Power Systems), *US 7078123B2*, **2006**.
[19] L. Wei, L. Zeng, M. C. Wu, X. Z. Fan, T. S. Zhao, *Appl. Energy* **2019**, *251*, 113344.
[20] K. Utsumi (Galaxy Co., Ltd.), *US 2015/0372331A1*, **2015**.
[21] W. Li, M. L. Perry (United Technologies Corporation), *US 2016/0093925A1*, **2016**.
[22] W. Li, R. Zaffou, C. C. Sholvin, M. L. Perry, Y. She, *ECS Trans.* **2013**, *53*, 93.
[23] A. Smeltz (United Technologies Corporation), *US 2018/0105944A1*, **2018**.
[24] C. Fan, *Int. J. Electrochem. Sci.* **2017**, 7728.
[25] K. Kanji Sato, I. Masato Nakajima (Sumitomo Electric Industries Ltd), *US 5368762A*, **1994**.
[26] M. Nakajima, T. Akahoshi, M. Sawahata, Y. Nomura, K. Sato (Kashima-Kita Electric Power Corporation), *US 5587132*, **1996**.
[27] K. Kampanatsan-Yakorn, P. Kachanadul (Squirrel Holdings Ltd.), WO 2013/027076A1, **2013**.

[28] J. Heo, J.-Y. Han, S. Kim, S. Yuk, C. Choi, R. Kim, J.-H. Lee, A. Klassen, S.-K. Ryi, H.-T. Kim, *Nat. Commun.* **2019**, *10*, 4412.
[29] H. Kaneko, A. Negishi, K. Nozaki (Kashima-Kita Electric Power Corporation), *US 5250158*, **1993**.
[30] M. Skyllas-Kazacos (Welsh & Katz Ltd.), *US 2004/0241552A1*, **2004**.
[31] M. Skyllas-Kazacos, J. F. McCann, *Advances in Batteries for Medium and Large-Scale Energy Storage*, Elsevier, Cambridge **2015**.
[32] M. Keshavarz, G. Zu (Imergy Power Systems Inc.), *US 2015/0050570A1*, **2015**.
[33] Y. Tanaka, K. Horikawa, M. Mita, N. Tokuda, M. Kubata (Sumitomo Electric Industries Ltd, Kansai Electric Power Co., Nippon Chemical Industrial Co.), *US 6613298B2*, **2003**.
[34] X.-W. Wu, S. Peng, B.-J. Feng, T. Yamamura, Y. Takashi, I. Satoh, S.-q. Liu, K.-L. Huang, *J. Inorg. Mater.* **2011**, *26*, 535.
[35] M. Dassisti, G. Cozzolino, M. Chimienti, A. Rizzuti, P. Mastrorilli, P. L'Abbate, *Int. J. Hydrogen Energy* **2016**, *41*, 16477.
[36] U.S. Geological Survey, Metal Prices in the United States through 2010, http://ubs.usgs.gov/sir/2012/5188/ (accessed: June 2020).
[37] Vanadium Price, http://www.vanadiumprice.com/ (accessed: April 2020).
[38] R. R. Moskalyk, A. M. Alfantazi, *Miner. Eng.* **2003**, *16*, 793.
[39] P. Buchholz, T. Brandenburg, *Chem. Ing. Tech.* **2018**, *90*, 141.
[40] F. Rahman, *PhD Thesis*, University of New South Wales **1998**.
[41] U. Kazuyuki, I. Hideyuki, S. Keiichi, *Anal. Sci.* **1991**, *7*, 115.
[42] W. D. Treadwell, R. Nieriker, *Helv. Chim. Acta* **1941**, *24*, 1098.
[43] S. Cherevko, S. Geiger, O. Kasian, N. Kulyk, J.-P. Grote, A. Savan, B. R. Shrestha, S. Merzlikin, B. Breitbach, A. Ludwig, K. J. J. Mayrhofer, *Catal. Today* **2016**, *262*, 170.
[44] P. J. Niebergall, G. Milosovich, J. E. Goyan, *J. Pharm. Sci.* **1963**, *52*, 236.
[45] A. Dokoumetzidis, P. Macheras, *Int. J. Pharm.* **2006**, *321*, 1.
[46] M. J. Habib, *Pharmaceutical Solid Dispersion Technology*, Technomic Publishing Co, Lancaster, UK **2001**.
[47] S. Asai, Y. Konishi, Y. Sasaki, *J. Chem. Eng. Japan* **1988**, *21*, 107.
[48] M. Kraume, *Transportvorgänge in der Verfahrenstechnik: Grundlagen und Apparative Umsetzungen*, Springer, Berlin **2004**.
[49] F. Steimle, R. Plank, *Handbuch der Kältetechnik*, Springer, Berlin **1988**.
[50] *VDI-Wärmeatlas: Mit 320 Tabellen*, 11th ed., Springer, Berlin **2013**.
[51] R. El Hage, F. Chauvet, B. Biscans, L. Cassayre, L. Maurice, T. Tzedakis, *Chem. Eng. Sci.* **2019**, *199*, 123.
[52] H. Al-Fetlawi, A. A. Shah, F. C. Walsh, *Electrochim. Acta* **2009**, *55*, 78.
[53] J. Siepmann, F. Siepmann, *Int. J. Pharm.* **2013**, *453*, 12.
[54] M. Bisrat, E. K. Anderberg, M. I. Barnett, C. Nyström, *Int. J. Pharm.* **1992**, *80*, 191.
[55] M. Ulaganathan, V. Aravindan, Q. Yan, S. Madhavi, M. Skyllas-Kazacos, T. M. Lim, *Adv. Mater. Interfaces* **2016**, *3*, 1500309.
[56] M. Weller, *Inorganic Chemistry*, 6th ed, Oxford University Press, Oxford **2014**.
[57] M. Tahir, L. Pan, F. Idrees, X. Zhang, L. Wang, J.-J. Zou, Z. L. Wang, *Nano Energy* **2017**, *37*, 136.
[58] Vanadyl-Sulphate Solution – Gesellschaft für Elektrometallurgie mbH, https://bit.ly/31MY7OI (accessed: July 2020).